Journal of Marine Science and Technology

Volume 27 | Issue 5 Article 7

Case Study for the Ground Motion Analyses and Seabed Soil Liquefaction Potential of Chang-Bin Offshore Wind Farm

Yu-Shu Kuo

Chi-Sheng Lin

Juin-Fu Chai

Yu-Wen Chang

Yu-Hsiu Tseng

Recommended Citation

Kuo, Yu-Shu; Lin, Chi-Sheng; Chai, Juin-Fu; Chang, Yu-Wen; and Tseng, Yu-Hsiu (2019) "Case Study for the Ground Motion Analyses and Seabed Soil Liquefaction Potential of Chang-Bin Offshore Wind Farm," *Journal of Marine Science and Technology*: Vol. 27: Iss. 5, Article 7.
DOI: 10.6119/JMST.201910_27(5).0007
Available at: https://jmstt.ntou.edu.tw/journal/vol27/iss5/7

Case Study for the Ground Motion Analyses and Seabed Soil Liquefaction Potential of Chang-Bin Offshore Wind Farm

Acknowledgements

The research was supported by the grants “Engineering databank and information modeling platform for offshore wind turbine foundation design and maintenance management (MOST 107-3113-E-006-011)”, the Ministry of Science and Technology of Taiwan.

Journal of Marine Science and Technology, Vol. 27, No. 5, pp. 448-462 (2019)
DOI: 10.6119/JMST.201910_27(5).0007

CASE STUDY OF THE GROUND MOTION ANALYSES AND SEABED SOIL LIQUEFACTION POTENTIAL OF CHANGBIN OFFSHORE WIND FARM

Yu-Shu Kuo[1], Chi-Sheng Lin[1], Juin-Fu Chai[2], Yu-Wen Chang[2], and Yu-Hsiu Tseng[3]

Key words: offshore wind farm, seabed soil liquefaction, ground motion analysis.

ABSTRACT

Evaluating seismic forces and soil liquefaction potential during the development of offshore wind farms in Taiwan is crucial. Wang et al. (2016) conducted a seismic hazard analysis and proposed a design earthquake response spectrum for the bedrock at the Changbin offshore wind farm. In this study, the recommended acceleration response spectrum was used to generate two design earthquakes (BH01_EW and BH01_NS) at the bedrock level that were compatible to the seismic characteristics of the Changbin offshore wind farm. The original soil data of borehole BH01(TORI) at the site were used to conduct a ground motion analysis and obtain design seismic surface forces. In engineering practice, simplified engineering soil profiles are commonly used to design foundations. The simplification of soil profiles causes uncertainties in the ground motion analyses. To determine the effects of soil profile simplification on design seismic loading, we established two engineering soil profiles for borehole BH01(TORI) and compared the ground motion analyses results. One of the simplified engineering soil profiles comprised a simplified profile of shear wave velocity distributed along the depth, whereas the other involved a simplified profile of soil unit weight along the depth. The soil profile with a simplified distribution of shear wave velocity engendered a significant underestimation of the maximum design seismic load at the seabed surface. The acceleration responses at the seabed level obtained from the ground motion analyses were used to evaluate the soil liquefaction potential at BH01(TORI) by employing the New Japan Road Association simplified empirical method. The results indicated a high potential of soil liquefaction in the seabed at the Changbin offshore wind farm, Taiwan. We observed more than 10-m-long liquefiable soil layers. A risk assessment of foundation stability loss due to soil liquefaction should be considered in offshore wind turbine foundation design.

I. INTRODUCTION

Seabed soil liquefaction is not an issue in the design process of European offshore wind farms because these offshore wind farms are not located in active seismic zones. However, seismic demands and seabed soil liquefaction should be considered in the foundation design of offshore wind turbines in offshore wind farms in Taiwan, which is located in the circumpacific seismic zone. The seabed soil of the potential offshore wind farms in Taiwan generally comprises layers of alluvial silt and sand. Soil liquefaction may occur during an earthquake and could result in loss of wind turbine foundation stability. Evaluations of the soil liquefaction potential and how it affects the behavior of wind turbines must be considered in the design of offshore wind turbine foundations in seismically active areas.

Seed et al. (1971), Tokimatsu and Yoshimi (1983), Robertson and Campanella (1985), Seed and DeAlba (1986), Ishihara and Kosecki (1989), Tokimatsu et al. (1991), Finn (1991), Japan Road Association (1996), and Andrus and Stokoe (2000) have proposed methods for evaluating soil liquefaction potential. These methods have been developed using onshore-based soil liquefaction cases and laboratory studies. The engineering method widely used to evaluate soil liquefaction potential is the simplified empirical method; this method is extensively used because of its easy application. To use the simplified empirical method, the peak ground acceleration (PGA) A_{max} of the design earthquake at the site of the offshore wind farm should be determined. However, a seismic design standard that can serve as a reference for

Paper submitted 04/01/9; revised 05/30/19; accepted 08/22/19. Author for correspondence: Yu-Shu Kuo (e-mail: kuoyushu@mail.ncku.edu.tw).
[1] Department of Hydraulic and Ocean Engineering, National Cheng Kung University, Tainan, Taiwan, R.O.C.
[2] National Center for Research on Earthquake Engineering, Taipei, Taiwan, R.O.C.
[3] ChengDa Environment and Energy Ltd., Taipei, Taiwan, R.O.C.

evaluating the soil liquefaction potential of an offshore wind farm in Taiwan is not available. According to the recommendations in the ISO19901-2 (2004) and API RP2EQ (2014) standards, the results of seismic hazard analyses that identify all potential seismic sources within 320 km of a site should be used to evaluate the influence level of each source and to create a seismic hazard curve that estimates the annual exceedance probability at the site. Wang et al. (2016) collected a large quantity of historical seismic data from sources in the Taiwan Strait and used them to construct seismic hazard curves for offshore wind farms in western Taiwan through seismic hazard analyses. They used the curves to propose values of the short period and 1-s-period horizontal spectral acceleration coefficients (S_S^D, S_1^D, S_S^M, S_1^M) for 475-year and 2500-year return-period design earthquakes.

When seismic forces are transmitted from the bedrock to the surface, they are influenced by site effects, including the effects of the soil between the bedrock and seabed surface, soil layer geometry, and sediment alluviation sequence. Engineers often use ground motion analyses to determine the seismic characteristics of each soil layer, including the ground surface. Athanasopoulos et al. (1999) used finite element methods to perform ground motion analyses to explore the soil layer amplification effect in Egion, Greece. Phanikanth et al. (2011) used ground motion analyses to explore the soil amplification effects in various cities in India. In addition, Hashash and Park (2001) used DEEPSOIL, a ground motion analysis program developed by the University of Illinois at Urbana-Champaign, to analyze the transmission of seismic vibrations through various soil layer thicknesses in the Mississippi embayment. Kwok et al. (2007) used DEEPSOIL to explore the influence of various seismic events and soil damping on seismic ground responses. Site effects influence seismic accelerations transmitted to the ground surface as well as soil liquefaction assessments. Ground motion analyses require the seismic input at the bedrock, thickness of each soil layer, density of soil, shear wave velocities of each soil layer, and dynamic properties of soil (shear modulus and damping). In this study, the soil data of borehole BH01(TORI) of the Changbin offshore wind farm in the Taiwan Strait were used to perform ground motion analyses. Wang et al. (2016) obtained an appropriate design earthquake response spectrum for the Changbin offshore wind farm by conducting probabilistic seismic hazard analyses. To obtain a seismic motion consistent with the hazard level of the Changbin offshore area as an input to the ground motion analyses, this study used a frequency-domain method to generate an artificial seismic motion (Kramer, 1996). We selected an actual ground motion whose response spectrum is similar to that suggested by Wang et al. (2016) and adjusted the Fourier amplitude spectrum gradually until the response spectrum was consistent with the target response spectrum.

Geotechnical experts generally create a simplified engineering soil profile with limited laboratory test results and in situ test results for designing the foundations of offshore wind turbines. The geotechnical parameters of each soil layer in the soil profile are usually provided. For soil layers with similar properties, the geotechnical parameters of each simplified soil layer are equal to the weighted average parameters according to the corresponding thicknesses of the component layers. However, the aforementioned process of determining the engineering soil profile may add some uncertainties in foundation design. Uncertainties pertaining to the unit weight of soil and shear wave velocity can lead to different results of ground motion responses and may induce very different results of seabed soil liquefaction potential. Fig. 1 presents the research concept of this study. Soil profiles determined using different simplified processes were used in a ground motion analysis performed through the DEEPSOIL program (Hashash et al., 2016); subsequently, the seabed soil liquefaction potential was analyzed for the Changbin offshore wind farm. This study also examined the effects of uncertainties regarding the soil unit weight and shear wave velocity of a simplified soil profile on the ground motion analysis and seabed soil liquefaction potential analysis.

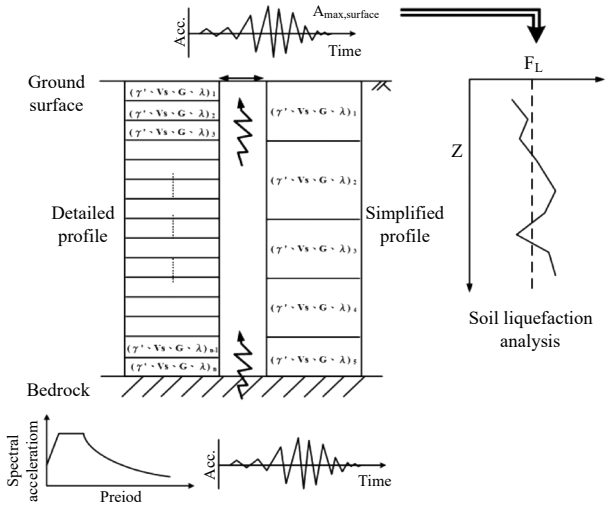

Fig. 1. Process of the ground motion analysis and soil liquefaction potential evaluation in this study

II. ONE-DIMENSIONAL GROUND MOTION ANALYSIS

When seismic waves are transmitted to the surface from the bedrock, the seismic characteristics are affected by the soil type, soil density, soil layer thickness, and soil layer sequence. A one-dimensional ground motion analysis is commonly used to estimate local site effects in engineering practice. In a one-dimensional ground motion analysis, soil layers are assumed to be stratified horizontally and underlain by a half space as the bottom layer (bedrock). Seismic waves are transmitted vertically through the soil layers. The propagation of harmonic waves that travel vertically through the horizontal soil layers can be described using the wave equation in Equation (1), where u is the horizontal displacement of the soil layer and

Table 1. Bedrock spectral acceleration coefficients of the Changbin offshore wind farm in Taiwan at oscillator periods of 0.3 and 1 s for the earthquake return periods of 475 and 2500 years (corrected to 1.5 standard deviations) (Wang et al., 2016)

Worksite	E	N	475 year		2500 year	
			S_S^D	S_1^D	S_S^M	S_1^M
BH01	175,290.1	2,656,259.6	0.68	0.37	1.11	0.64
BH02	172,724.6	2,652,211.9	0.66	0.37	1.09	0.63

is a function of depth z and time t and ρ is the soil density. The relationship between angular frequency ω, shear modulus G, viscosity η, and soil damping ratio ξ is expressed in Equation (2). The wave equation can be solved through separation of variables such that the soil displacement can be expressed as the product of functions of displacement and time, as shown in Eq. (3). By substituting Eq. (3) into Eq. (1), we obtain a standard differential equation with a single displacement variable. Subsequently, the general solutions for the wave equation presented in Eq. (4) and Eq. (5) are obtained. In Eq. (4), E and F are undetermined coefficients. The theory of ground motion analysis can be found in the studies by Schnabel et al. (1972), Kramer (1996), and Yoshida (2015).

$$\rho\frac{\partial^2 u}{\partial t^2}=G\frac{\partial^2 u}{\partial z^2}+\eta\frac{\partial^3 u}{\partial z^2\partial t} \tag{1}$$

$$\omega\eta = 2G\xi \tag{2}$$

$$u(z,t)=U(z)\cdot e^{i\omega t} \tag{3}$$

$$u(z,t)=Ee^{i(kz+\omega t)}+Fe^{-i(kz-\omega t)} \tag{4}$$

$$k^2=\frac{\rho\omega^2}{G+i\omega\eta} \tag{5}$$

1. Seismic Motion Input

Ground motion analyses require using the time series of seismic accelerations in a particular soil layer as input motions. For the input motions, three types of acceleration time series can be considered: (1) time series of representative earthquakes that have occurred near the work site, (2) time series of a historical earthquake selected by the designer, and (3) artificial acceleration time series generated from the design seismic response spectrum. For the study area, namely the Changbin offshore wind farm, no representative historical record of earthquake events exists. Due to the lack of an ocean-bottom seismometer in the Taiwan Strait, time series (1) and (2) were not considered in this study. Wang et al. (2016) conducted a seismic hazard analysis for the Changbin offshore wind farm at borehole BH01(TORI), and the results are presented in Table 1 and Fig. 2. The recommended seismic acceleration response spectra are displayed in Fig. 3. The present study used the recommended seismic response spectrum provided by Wang et al. (2016) to set up artificial design earthquake data as input for the ground motion analysis. To simultaneously reflect the seismic hazards and surface motion characteristics at the Changbin offshore wind farm, a real acceleration time series whose response spectrum is similar to that proposed by Wang et al. (2016) was selected, and the Fourier amplitude spectrum was gradually adjusted until the response spectrum of the acceleration time series was consistent with the target response spectrum. Thus, we obtained the artificial acceleration time series for the design earthquakes at the site of the offshore wind farm.

2. Soil Profiles

A soil profile must be set up to perform a ground motion analysis. Inputs such as thickness, unit weight ρ, and shear wave velocity V_s or shear modulus G are required for each soil layer. The shear wave velocity and shear modulus can be interconverted using Eq. (6). The standard penetration test (SPT) is conventionally used for offshore soil investigation to obtain the in situ engineering properties of soil in Taiwan. The SPT is performed at intervals of 1.5 to 3 m along the depth. Split spoon soil samples (disturbed sample) are also taken to a laboratory to determine the basic physical properties of the soil. In engineering practice, foundation design relies on the engineering soil profile, which is created based on SPT results and might depend on engineering assessments. The soil parameters of each soil layer in the engineering soil profile can be determined using the weighted average of the parameters based on the thicknesses of layers obtained from laboratory tests conducted on split spoon samples. In a ground motion analysis, ground motion responses are affected by soil unit weight and shear wave velocity directly. In situ shear wave velocity records are not available near the Changbin offshore wind farm. Therefore, the present study obtained shear wave velocities from the maximum shear modulus presented in Eq. (6). The maximum shear modulus of soil is affected by the void ratio e, mean effective stress σ_m', and overconsolidation ratio (OCR). The recommendations of Hardin and Richart (1963), Seed and Idriss (1970), Hardin and Drnevich (1972), Iwasaki and Tatsuoka (1977), Hardin (1978), Jamiolkowski et al. (1991), and DNV (2002) can be used to calculate the

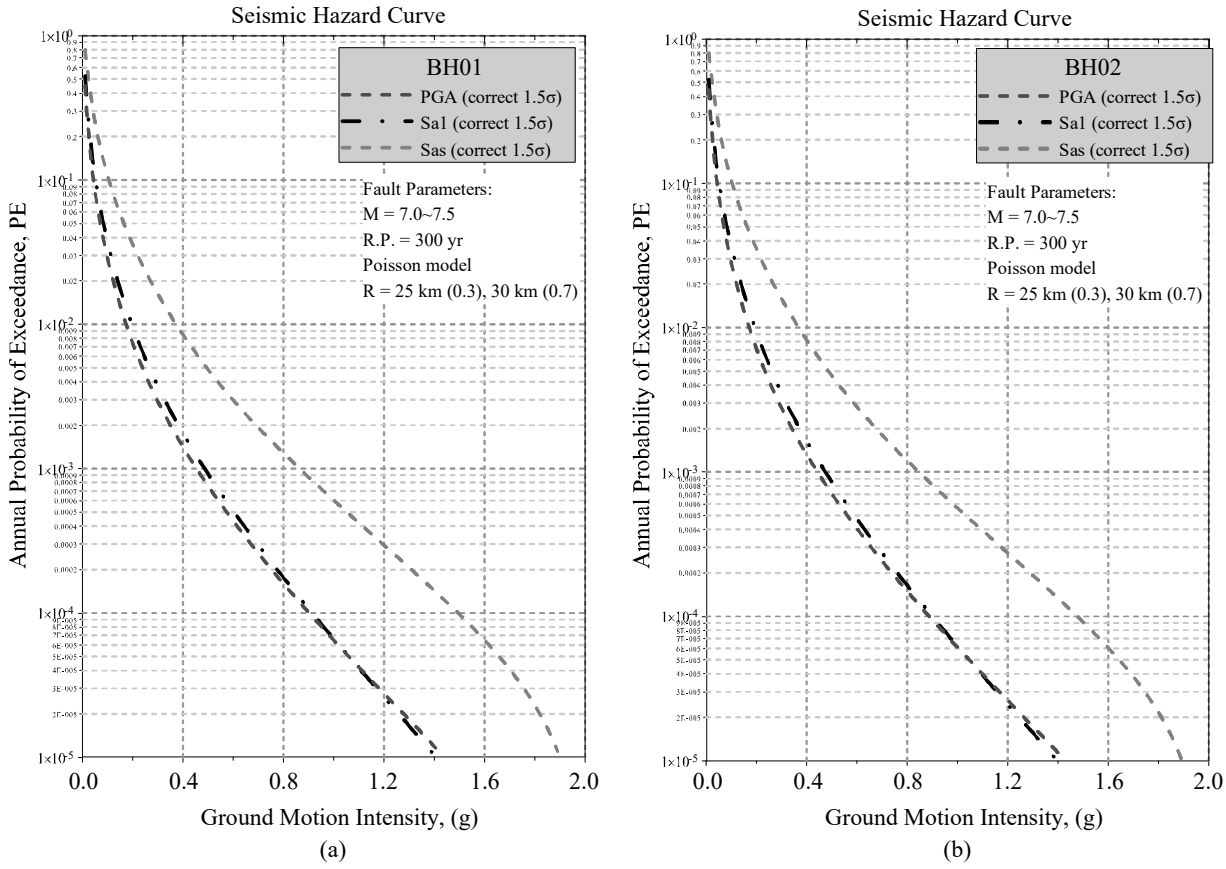

Fig. 2. The PSHA analysis results at the location in the Chang-Bin offshore wind Farm: (a) BH01(TORI); (b) BH02(TORI) (Wang et al., 2016)

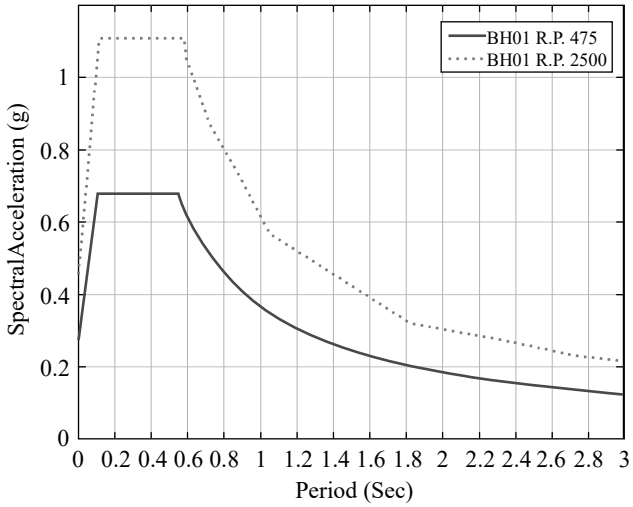

Fig. 3. Earthquake acceleration response spectra of the Changbin offshore wind farm, Taiwan (Wang et al., 2016)

maximum shear modulus of soil G_{max}. According to the offshore wind turbine design standard DNV (2002), the maximum shear modulus (kPa) can be calculated using Eq. (7) for cohesive or noncohesive soil. The value of the semiempirical coefficient A ranges from 2000 to 4000 according to the soil conditions. The value of the OCR is 1 for sandy soil and normally consolidated clay. The parameter k is the OCR index that is related to the plastic index, as shown in the study by Hardin and Drnevich (1972).

$$V_s = \sqrt{\frac{G_{\max}}{\rho}} \tag{6}$$

$$G_{\max} = A\frac{(3-e)^2}{1+e}\sqrt{\sigma_m'}\,(OCR)^k \tag{7}$$

3. Dynamic Properties of Soil

The stress–strain responses of soil are nonlinear. As the shear strain γ of soil increases, the shear modulus decreases and the damping ratio increases. Changes in the soil shear modulus and damping ratio with shear strain can be determined by conducting the resonant column test, bender element test, dynamic triaxial test, and dynamic simple shear test. These tests are applicable within a certain range of shear strains. The resonant column and bender element tests are mainly used to determine the soil properties under small-strain ($\gamma < 10^{-3}$) conditions. The dynamic triaxial and dynamic simple shear tests are suitable for determining the soil properties

under moderate shear strain ($\gamma \geq 10^{-3}$). Seed and Idriss (1970), Silver and Seed (1971), Vucetic and Dobry (1991), Ishibashi (1992), Smoltczyk (2001), and DNV (2002) have presented the recommended ranges of the dynamic properties of various types of soil. Hardin and Drnevich (1972) proposed the use of hyperbolic functions to describe the shear modulus attenuation and damping ratio changes with an increase in the shear strain (Eqs. (8)-(10)). Engineers can obtain the reference dynamic properties of soil using the suggestion of Hardin and Drnevich (1972).

$$\frac{G}{G_{\max}} = \frac{1}{1+\frac{G_{\max}\cdot\gamma}{\tau_{\max}}} \tag{8}$$

$$\xi = \frac{\xi_{\max}\cdot\frac{G_{\max}\cdot\gamma}{\tau_{\max}}}{1+\frac{G_{\max}\cdot\gamma}{\tau_{\max}}} \tag{9}$$

$$\tau_{\max} = \left[\left(\frac{1+K_0}{2}\sigma_v'\sin\phi' + c'\cos\phi'\right)^2 - \left(\frac{1-K_0}{2}\sigma_v'\right)^2\right]^{1/2} \tag{10}$$

$$K_0 = \begin{cases} 1-\sin\phi' & \text{for sand} \\ 0.44+0.0042PI & \text{for clay} \\ K_{0,OCR} = K_0\cdot\sqrt{OCR} & \text{for over consolidated clay} \end{cases} \tag{11}$$

In Eqs. (8)-(10), G is the shear modulus of soil under various shear strain conditions; τ_{max} is the shear strength associated with the initial effective stress; ξ_{max} is the damping ratio of soil under a large shear strain; K_0 is the coefficient of earth pressure at rest, which can be calculated using Eq. (11); σ_v' is the vertical effective stress; ϕ' is the effective internal friction angle; and c' is cohesion. This study substituted the soil unit weight, cohesion, and effective friction angle obtained from each soil layer in borehole BH01(TORI) into Eq. (8)-(11) to obtain the dynamic properties of soil.

III. SIMPLIFIED EMPIRICAL METHOD FOR SOIL LIQUEFACTION

In engineering practice, the simplified empirical method is commonly used to calculate the factor of safety against soil liquefaction F_L. The actor of safety against liquefaction is defined as the ratio between the cyclic resistance ratio $(\tau/\sigma_v')_R$ of soil and the externally applied cyclic stress ratio $(\tau/\sigma_v')_L$, as expressed in Eq. (12). When F_L is higher than 1, soil liquefaction does not occur during a seismic event. If F_L is less than 1, soil liquefaction may occur during an earthquake.

$$F_L = \frac{(\tau/\sigma_v')_R}{(\tau/\sigma_v')_L} \tag{12}$$

The cyclic resistance ratio $(\tau/\sigma_v')_R$ of soil can be determined using the in situ SPT-N value according to the methods recommended by Seed et al. (1975, 1979, 1985), Ishihara and Koseki (1989), Koester (1994), the Japan Road Association (1996), and Tokimatsu and Yoshimi (1983). The cyclic resistance ratio can be determined using cone penetration tests or in situ shear wave velocity measurements according to the methods proposed by Robertson and Campanella (1985), Seed and DeAlba (1986), Olsen (1997), Robertson and Wride (1998), Tokimatsu et al. (1991), Finn (1991), and Andrus and Stokoe (2000).

To evaluate soil liquefaction potential, the present study used the New Japan Road Association (NJRA) simplified empirical method recommended in "Seismic Design Specifications and Commentary of Buildings" for onshore buildings in Taiwan. In the NJRA method, the earthquake-induced cyclic stress ratio $(\tau/\sigma_v')_L$ is calculated using Eq. (13). Here, A_{max} is the PGA (gravitational acceleration g) and r_d is the reduction factor of the peak shear stress in the direction of depth and is calculated using Eq. (14).

$$(\tau/\sigma_v')_L = r_d\cdot A_{\max}\cdot\frac{\sigma_v}{\sigma_v'} \tag{13}$$

$$r_d = 1-0.015z \tag{14}$$

The cyclic resistance ratio $(\tau/\sigma_v')_R$ in the NJRA method is calculated using Eq. (15), where c_w is the corrected seismic force coefficient. Small to moderate earthquakes (return period of 30 years) and design earthquakes (return period of 475 years) in hidden plate boundaries have a c_w of 1. For design earthquakes (return period of 475 years) directly above inland faults, c_w is calculated using Eq. (16). The triaxial strength ratio R_L is calculated from the results of SPTs, as shown in Eq. (17).

$$(\tau/\sigma_v')_R = c_w\cdot R_L \tag{15}$$

$$c_w = \begin{cases} 1.0 & , R_L \leq 0.1 \\ 3.3R_L+0.67 & , 0.1 < R_L \leq 0.4 \\ 2.0 & , 0.4 < R_L \end{cases} \tag{16}$$

$$R_L = \begin{cases} 0.0882\sqrt{\frac{N_a}{1.7}} & , N_a < 14 \\ 0.0882\sqrt{\frac{N_a}{1.7}} + 1.6\times10^{-6}\cdot(N_a-14)^{4.5} & , 14 \leq N_a \end{cases} \tag{17}$$

where N_a is the SPT result corrected using overburden stress and fine content (FC). The NJRA method recommends the use of Eq. (18) to calculate N_a for sandy soil, where N_1 is the result

of the SPT corrected using overburden stress by using Eq. (19). Moreover, c_1 and c_2 are FC correction factors calculated using Eq. (20) and (21), respectively.

$$N_a = c_1 N_1 + c_2 \tag{18}$$

$$N_1 = \frac{1.7N}{(\sigma_v^{'} / p_a + 0.7)} \tag{19}$$

$$c_1 = \begin{cases} 1 & , 0\% \le \mathrm{FC} < 10\% \\ (\mathrm{FC}+40)/50 & , 10\% \le \mathrm{FC} < 60\% \\ (\mathrm{FC}/20)-1 & , 60\% \le \mathrm{FC} \end{cases} \tag{20}$$

$$c_2 = \begin{cases} 0 & , 0\% \le \mathrm{FC} < 10\% \\ (\mathrm{FC}-10)/18 & , 10\% \le \mathrm{FC} \end{cases} \tag{21}$$

IV. GROUND MOTION ANALYSIS AT BH01(TORI) OF CHANGBIN OFFSHORE WIND FARM

This study conducts ground motion analysis on the borehole BH01(TORI) in the Changbin wind farm. Detailed information on the soil layer in the borehole was obtained from the Changbin seabed soil ground investigation report (TORI, 2012). In this section, we present the input soil conditions for the ground motion analysis at BH01(TORI).

1. Soil Profile at the Borehole BH01(TORI) for Ground Motion Analysis

BH01(TORI) is located 5 km off the coast of Changhua (E175290.1, N2656259.6), Taiwan (Fig. 4), and the water depth here is 19.75 m. The soil data of BH01(TORI) is provided in the Appendix. The seabed soil in the western offshore area of Taiwan is Quaternary alluvium. Due to the effects of waves, currents, and river alluviation, the soil condition of the seabed surface soil is mostly loose. In the Changbin offshore wind farm area, the soil profile at a depth of 0 to 40 m and a depth deeper than 65 m is mainly silty sand with thin layers of low-plasticity silty clay. At a depth between 40 and 65 m, sand and clay are deposited layer by layer. In situ testing results revealed that within 10 m of the seabed surface, the soil condition is loose to medium dense, with the corresponding SPT-N values being less than 15. At depths greater than 10 m, the soil was determined to be generally medium-dense to dense sand, with the corresponding SPT-N values being larger than 20. The highest SPT-N value was 48. The soil unit weight was measured to be between 17.36 and 21.48 kN/m^3. The void ratio was also calculated to range from 0.4 to 1.02.

To determine the soil profile for the one-dimensional ground motion analysis, the detailed field investigation data obtained for BH01(TORI) were used in this study. The

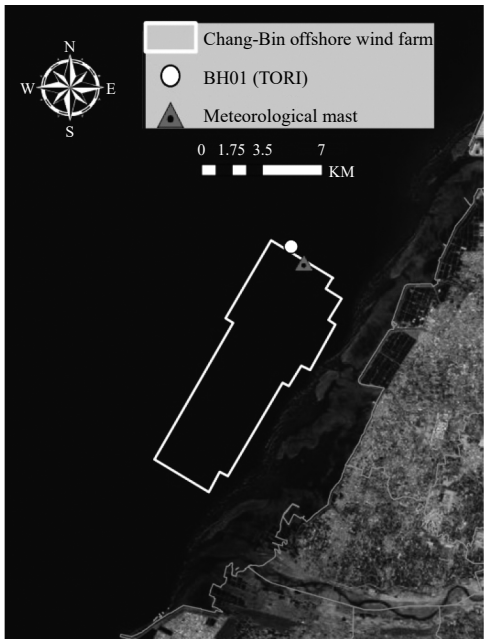

Fig. 4. Location of the Changbin offshore wind farm and the borehole BH01(TORI)

detailed soil profile was determined from soil samples in a split tube and was observed to contain 52 layers of soil, with the thickness of each soil layer ranging from 1.25 to 2.55 m. Fig. 5(a) shows this detailed soil profile, hereafter referred to as profile A. In profile A, the unit weight of soil is shown to range from 17.36 to 21.48 kN/m^3. The soil shear wave velocity generally increases with depth and ranges from 94 to 369 m/s.

In practice, engineers simplify the soil profile by combining soil layers with similar engineering properties. The geotechnical parameters of the simplified soil profiles are provided after obtaining the weighted average of the soil parameters based on the thickness of each soil layer. This simplified soil profile is generally considered in foundation design processes. The result of soil simplification may vary due to different personnel judgments or different design applications. In this study, first, the SPT-N values of all detailed layers were used to judge the simplification of the soil layers. If adjacent detailed layers were determined to have a similar SPT-N value, they were classified as the same soil layer. Second, the soil was roughly classified into three types—sand, silt, and clay. Based on the simplified soil layer from step one, if adjacent detailed layers were determined to have the same soil type, they were further classified as one simplified layer. To reduce the complexity of the soil profile, thin layers with a thickness lower than 2 m were combined into adjacent thick layers. A detailed soil profile and simplified soil profile were adopted in the ground motion analysis in this study, and the effects of soil unit weight and soil shear wave velocity were quantified.

Regarding the simplified soil profile, 52 soil layers were simplified into a soil profile with six layers. BH01(TORI) was determined to have five sandy soil layers (soil layer I, II, III,

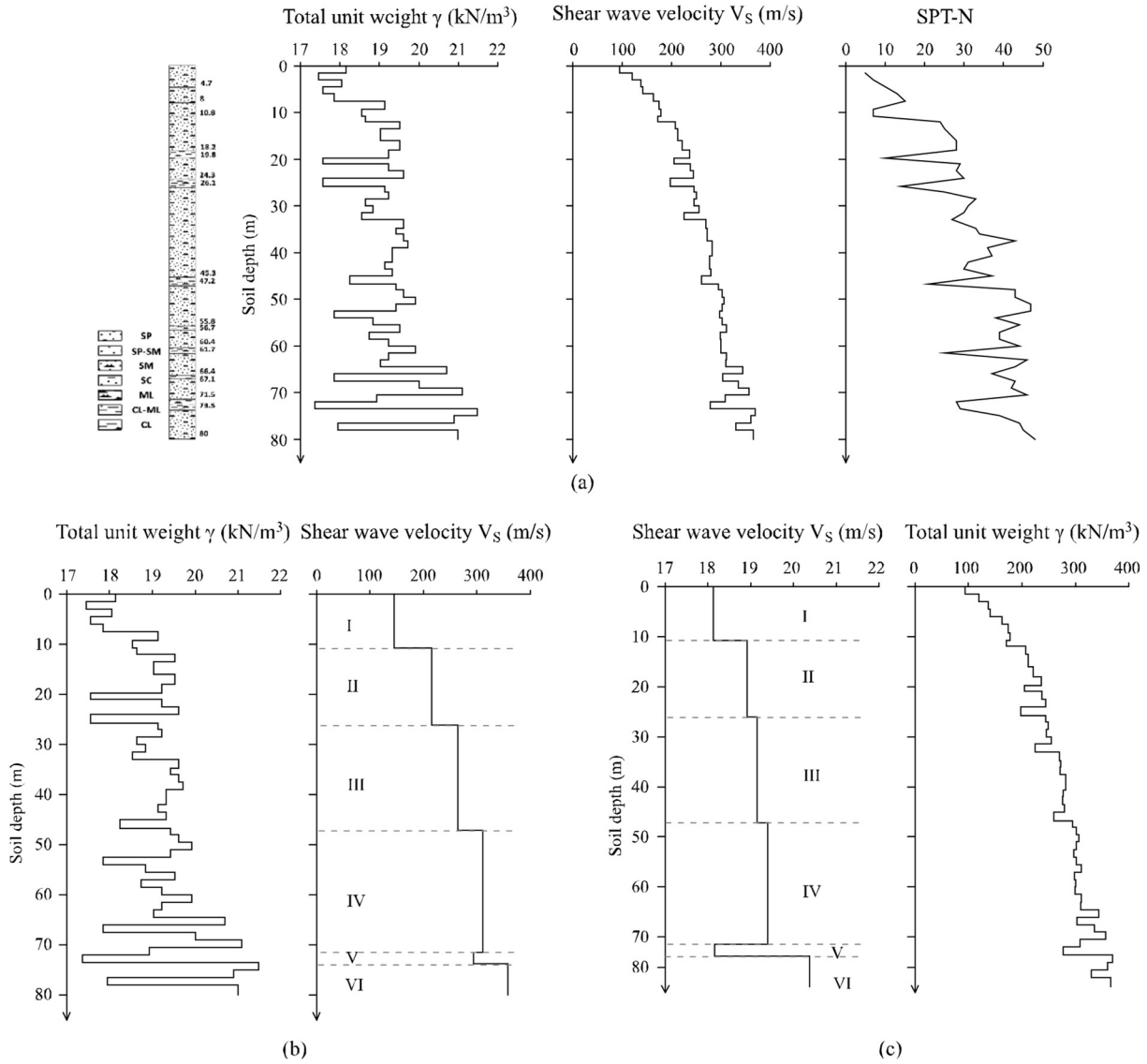

Fig. 5. Soil profiles of BH01(TORI) used for ground motion analysis: (a) Soil profile A (52 soil layers with detailed soil unit weight and detailed shear wave velocity); (b) Soil profile B (detailed soil unit weight profile combined with shear wave velocity profile simplified along the depth); (c) Soil profile C (soil unit weight profile simplified along the depth combined with a detailed shear wave velocity profile)

IV, and VI) and one clayey soil layer (soil layer V). The soil unit weights of the six soil layers were calculated to range from 18.13 to 20.38 kN/m^3, and the shear wave velocities were derived to range from 144 to 357 m/s. Two simplified soil profiles were considered in this study. Soil profile B represented the soil profile whose soil unit weight was obtained from the detailed soil profile. An averaged shear wave velocity was derived for soil profile B (Fig. 5(b)). By contrast, an average soil unit weight was determined for soil profile C according to the simplified soil profile and the shear wave velocity of the detailed soil profile (Fig. 5(c)). The methods presented in Sections II.2 and II.3 were used to determine the shear modulus and damping ratio of each soil layer in soil profile A, soil profile B, and soil profile C, as shown in Fig. 6. The A value in Equation (7) was set as 3000 to determine the maximum shear modulus. The maximum damping ratio ξ_{max} was determined from the results of cyclic simple shear tests of the soil obtained from the Changbin offshore wind farm. The test results are shown in Fig. 7. Based on the test results, the maximum damping ratio ξ_{max} of 20% was used in this study.

2. Seismic Motions at the Bedrock of the Changbin Offshore Wind Farm

Wang et al. (2016) recommended the design earthquake response spectrum of the bedrock at BH01(TORI) in the Changbin offshore wind farm. In this study, the frequency-domain method was used to generate two artificial seismic acceleration time series matching the ground motion characteristics of the Changbin offshore wind farm. We selected an actual ground motion with a similar response spectrum to that suggested by

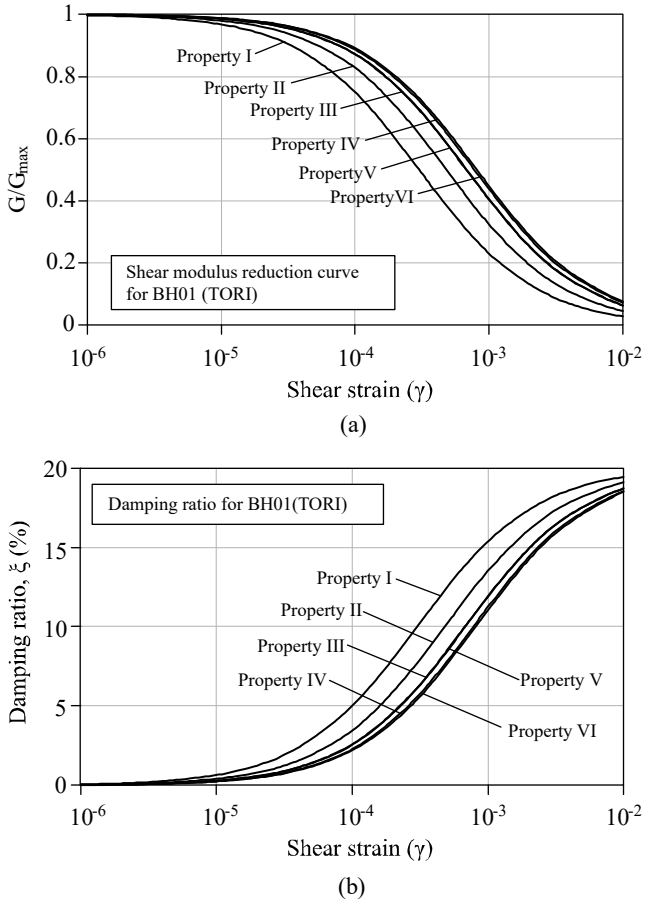

Fig. 6. Shear modulus and damping ratio of each engineering soil layer of BH01(TORI)

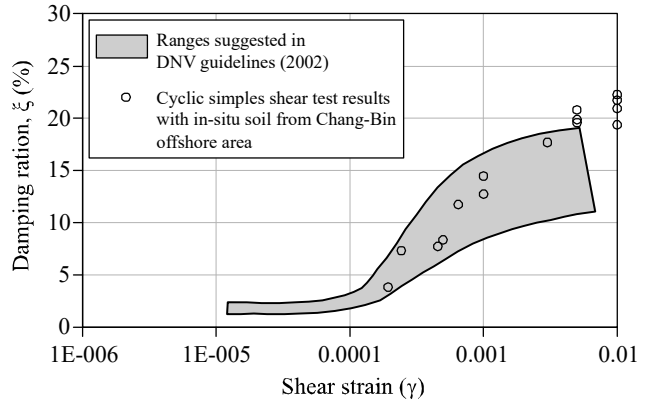

Fig. 7. Damping ratio of soil in Changbin offshore wind farm determined from cyclic simple shear tests

Wang et al. (2016), and we adjusted the Fourier amplitude spectrum gradually until the response spectrum was consistent with the target response spectrum. We used these artificial earthquake acceleration time series as input for the reference layer (bedrock) to conduct our ground motion analysis. Fig. 8 presents the acceleration time series and response spectra of

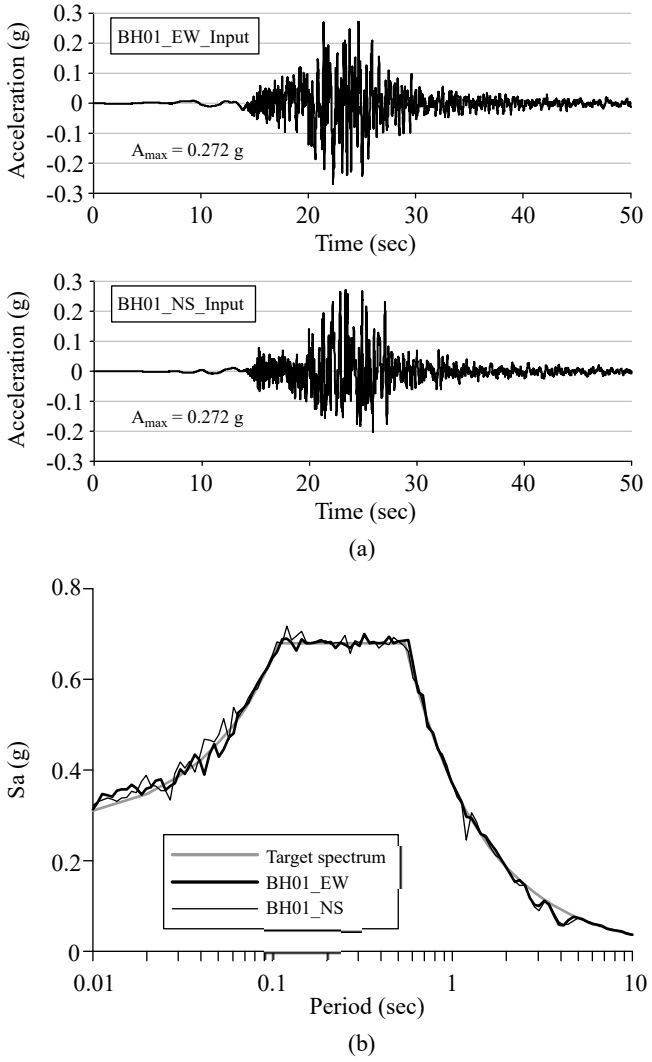

Fig. 8. Seismic acceleration time series and acceleration response spectra of artificial earthquakes in the present study

the artificial earthquakes BH01_EW and BH01_NS. The value of peak acceleration A_{max} is equal to the value of the spectral acceleration coefficient corresponding to a period of 0 s. For the location of BH01(TORI), the A_{max} value of input motion was determined to be 0.272*g* according to the design earthquake response spectrum.

According to the regulation "Seismic Design Specifications and Commentary of Buildings," the bedrock must have an average shear wave velocity $V_{s,30}$ (weighted average shear wave velocity of soil layers with a depth of 30 m) of more than 360 m/s. In this study, the shear wave velocity of each soil layer in BH01(TORI) was calculated using Eqs. (6) and (7). The shear wave velocity of soil presented in Fig. 5(a) indicates the existence of no bedrock within 80 m below the seabed of the Changbin offshore wind farm. Due to limited information of the soil layer in the Changbin offshore wind farm, a reference bedrock was considered as bedrock at the depth of 80 m (the bottom of borehole BH01) beneath the seabed in this study.

Table 2. Considerations of scenarios of seismic ground motion analyses

Case number	Ground motion analysis input conditions		
	Unit weight and shear wave velocity profile	Dynamic properties (Fig. 6)	Seismic acceleration time series (Fig. 8(a))
1	Soil profile A (Fig. 5(a))	Each engineering soil layer corresponding to one dynamic property	BH01_EW
2			BH01_NS
3	Soil profile B (Fig. 5(b))		BH01_EW
4			BH01_NS
5	Soil profile C (Fig. 5(c))		BH01_EW
6			BH01_NS

Table 3. Comparison of peak accelerations of input motion with those of motion at the seabed surface obtained from ground motion analysis for soil profile A (Fig. 5(a))

Earthquake	Peak acceleration of the input motion $A_{max,input}$ (g)	Peak ground acceleration $A_{max,surface}$ (g)	Amplification factor $A_{max,surface}/A_{max,input}$
BH01_EW	0.272	0.295	1.085
BH01_NS	0.272	0.209	0.768

V. GROUND MOTION ANALYSES FOR CHANGBIN OFFSHORE WIND FARM

The dynamic soil properties presented in Fig. 6 are specified in the soil profile in Fig. 5; these properties were integrated with design earthquakes (Fig. 8) to analyze seismic ground responses under a design earthquake. Table 2 presents the scenarios of our ground motion analysis that involved different boundary conditions and considered the uncertainties of soil parameters (soil unit weight and shear wave velocity).

1. Ground Motion Analysis Results of the Changbin Offshore Wind Farm at the Borehole BH01(TORI)

The results of the one-dimensional ground motion analysis of BH01(TORI) are presented in Fig. 9, Fig. 10, and Table 3. Fig. 9 presents a comparison of the acceleration time series of the input motion at the bedrock and those of the motion at the seabed surface due to the design earthquakes presented in Fig. 8. The vibration of the acceleration time series at the seabed surface was more moderate than that at the bedrock. This can be attributed to the reflection and dissipation of the high-frequency wave components during the wave propagation process. Table 3 shows a comparison of the peak accelerations of the input motions $A_{max,input}$ with those of the seabed surface $A_{max,surface}$ due to the design earthquakes. The maximum acceleration of the input earthquakes at the reference bedrock was 0.272*g*. The PGA $A_{max,surface}$ obtained through earthquake BH01_EW was 0.295*g*. The acceleration amplification factor $A_{max,surface}/A_{max,input}$ was 1.085. The PGA obtained through earthquake BH01_NS was 0.209*g*. The acceleration amplification factor was 0.768. These results reveal that even if the acceleration response spectra were the same, the differences in the phase spectrum between the input earthquakes (BH01_EW and BH01_NS) could lead to an amplification factor higher or lower than 1.

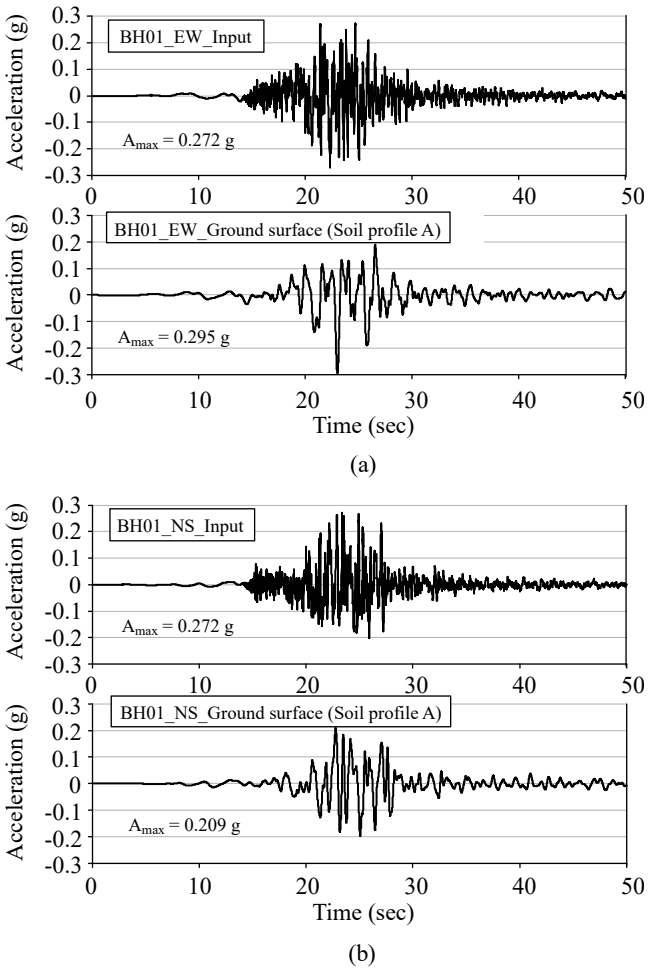

Fig. 9. Comparison of acceleration time series of input motion at the bedrock with those of motions at the seabed level obtained from ground motion analysis using soil profile A (Fig. 5(a))

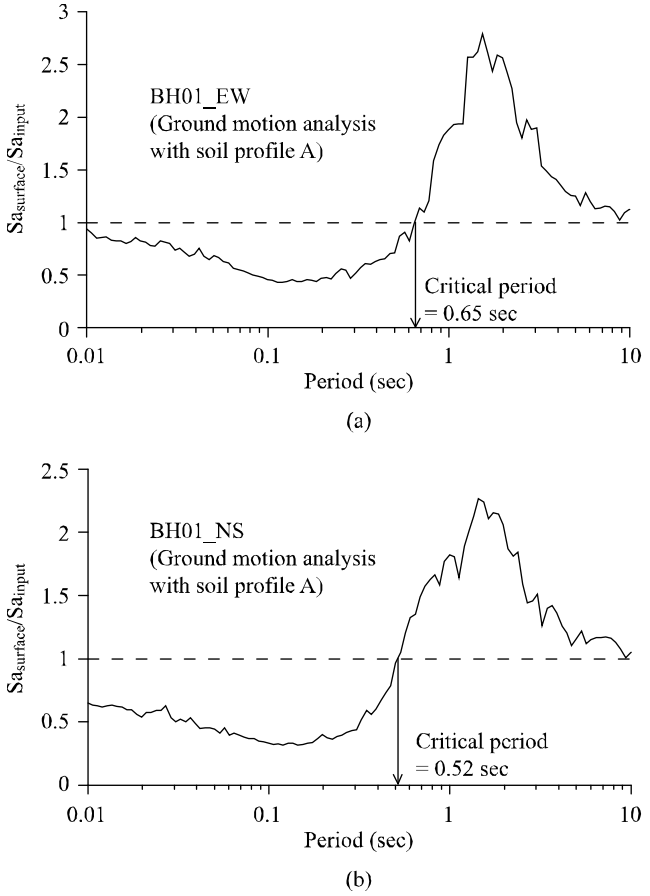

Fig. 10. Ratio of the spectral acceleration coefficient at the ground surface to the spectral acceleration coefficient of the input motion (ground motion analyses were performed using soil profile A, Fig. 5(a)): (a) artificial earthquake BH01_EW and (b) artificial earthquake BH01_NS

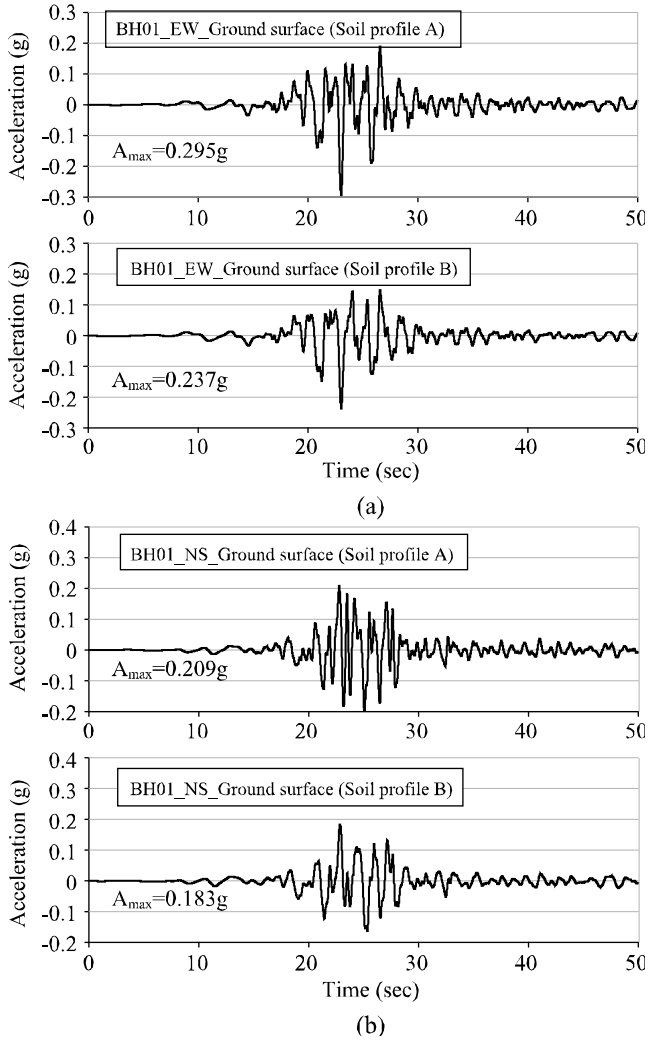

Fig. 11 Comparison of seabed surface acceleration time series obtained using ground motion analysis conducted using soil profile A (detailed soil profile) and soil profile B (detailed soil unit weight profile combined with shear wave velocity profile simplified along the depth)): (a) BH01_EW earthquake and (b) BH01_NS earthquake

To determine site effects on the spectral acceleration coefficient, this study divided the spectral acceleration coefficient at the ground surface ($Sa_{surface}$) by the coefficient of the input motion at the bedrock (Sa_{input}). The results are shown in Fig. 10. The $Sa_{surface}/Sa_{input}$ values corresponding to the short period were lower than 1, indicating that the site effects at BH01(TORI) could engender a decrease in the seismic response when a seismic wave is transmitted to the ground. For the period longer than the critical period, the $Sa_{surface}/Sa_{input}$ values were higher than q. For earthquake BH01_EW, the critical period was 0.65 s; the smallest $Sa_{surface}/Sa_{input}$ value was 0.441, and the largest value was 2.791, corresponding to a period of 1.54 s. For earthquake BH01_NS, the critical period was 0.52 s; the smallest $Sa_{surface}/Sa_{input}$ value was 0.313, and the largest value was 2.268, corresponding to a period of 1.44 s. Structures with long Eigen periods such as wind turbines are particularly susceptible to exacerbated seismic responses.

2. Effect of Uncertainties of Soil Unit Weight and Shear Wave Velocity on the Results of Ground Motion Analysis

Soil profile B (Fig. 5(b)) with a simplified profile of shear wave velocity and soil profile C (Fig. 5(c)) with a simplified profile of soil unit weight were used in the ground motion analysis to explore the effects of the uncertainties of soil properties on the analysis results. The design earthquakes—BH01_EW and BH01_NS—presented in Fig. 8 were used in the ground motion analysis, and the analysis results are compared with the results shown in Figs. 9 and 10.

The seabed surface acceleration time series that were obtained from the ground motion analysis conducted using soil profiles A, B, and C under the design earthquakes were compared, as presented in Figs. 11 and 12. The PGA obtained from the ground motion analysis conducted using soil profile A under BH01_EW was 0.295*g*. When soil profile B was used, the PGA was 0.237*g*, indicating a 19.7% reduction. When soil

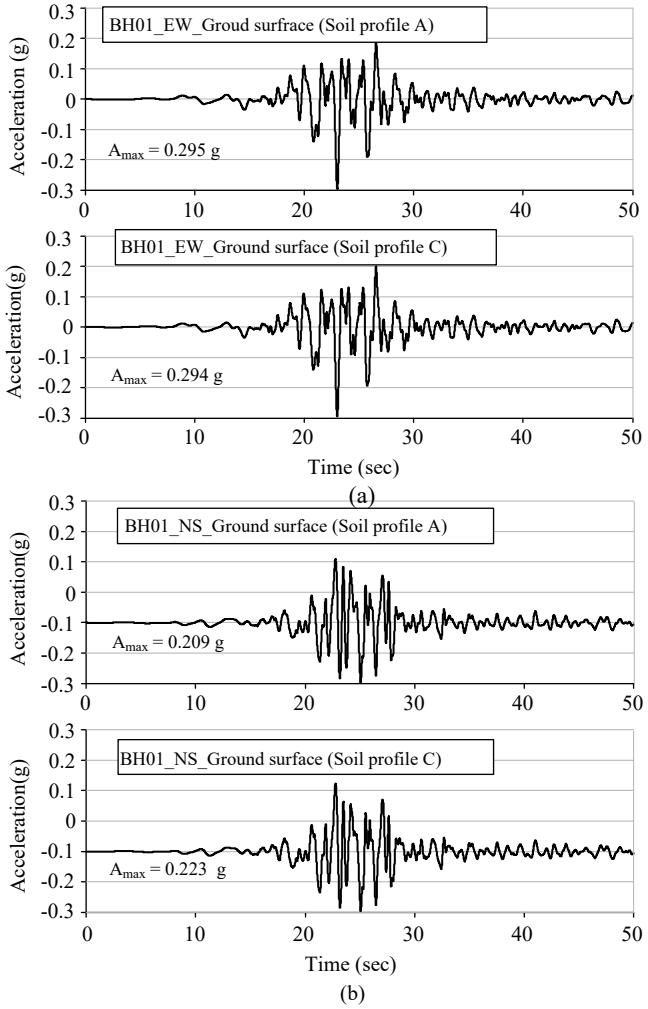

Fig. 12. Comparison of the seabed surface acceleration time series obtained from ground motion analysis conducted using soil profile A (detailed soil profile) and soil profile C (soil unit weight profile simplified along the depth combines with detailed shear wave velocity profile): (a)BH01_EW earthquake (b)BH01_NS earthquake

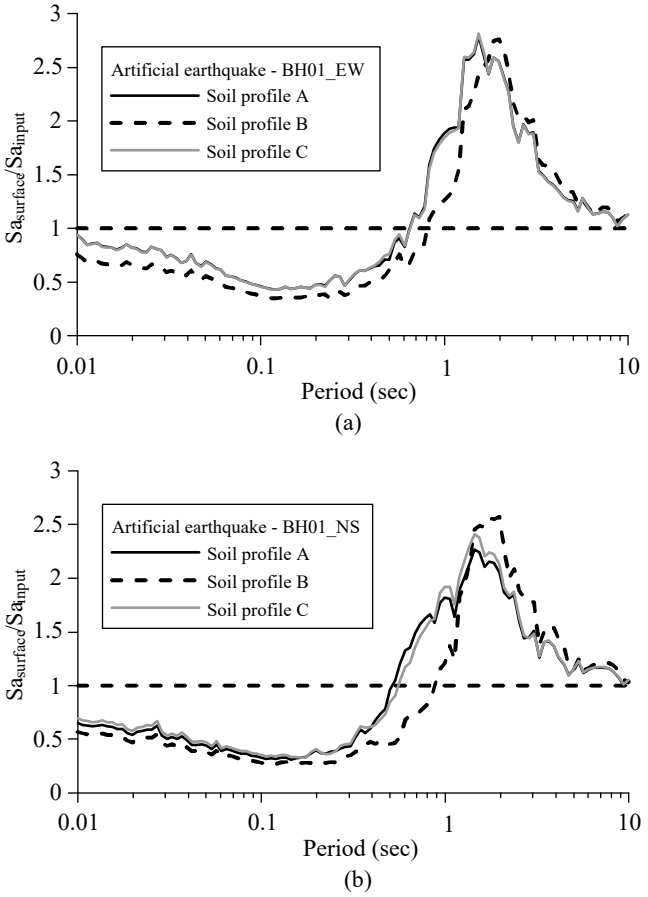

Fig. 13. Effect of simplification of soil unit weight and shear wave velocity along depth on spectral acceleration coefficients: (a) artificial earthquake BH01_EW and (b) artificial earthquake BH01_NS

profile C was used, the PGA was 0.294*g*, indicating a slight 0.3% reduction. Under BH01_NS, the PGA obtained using soil profile A was 0.209*g*. When soil profile B was used, the PGA was 0.183*g*, signifying a 12.4% reduction. When soil profile C was used, the PGA was 0.223*g*, reflecting a 6.7% increase. The PGA comparison results (Figs. 11 and 12) show that when we used the soil profile with a simplified profile of shear wave velocity along the depth as the input for the ground motion analysis, the PGA was underestimated. However, when we used the simplified profile of soil unit weights along the depth, the PGA could be increased or decreased, depending on the input design earthquake.

The $Sa_{surface}/Sa_{input}$ values were calculated to determine the effects of simplification of soil unit weight and shear wave velocity along the depth on the spectral acceleration coefficients. Figs. 13(a) and 13(b) illustrate the results of the ground motion analyses conducted using BH01_EW and BH01_NS, respectively. As shown in the figures, regardless of the soil profile used, the trends of the distributions of the $Sa_{surface}/Sa_{input}$ values along with period remained the same. However, the simplification of the soil parameters in the ground motion analysis could result in different $Sa_{surface}/Sa_{input}$ values. As shown in Fig. 13(a), when soil profile B was used in the ground motion analysis, the $Sa_{surface}/Sa_{input}$ values for period shorter than 1.68 s were lower than those obtained from the ground motion analysis conducted using soil profile A. When soil profile C was used, the response spectrum was nearly identical to the responses obtained from the ground motion analysis conducted soil profile A. As presented in Fig. 13(b), when soil profile B was used, the $Sa_{surface}/Sa_{input}$ values for periods shorter than 1.3 s were lower than those obtained from the ground motion analysis conducted using soil profile A. When soil profile C was used, the $Sa_{surface}/Sa_{input}$ values were lower for periods that ranged between 0.4 and 0.9 s but were higher for periods that ranged between 0.9 and 2.0 s when compared with the values obtained from the ground motion analysis conducted using soil profile A.

In the ground motion analysis, the soil profile with a sim

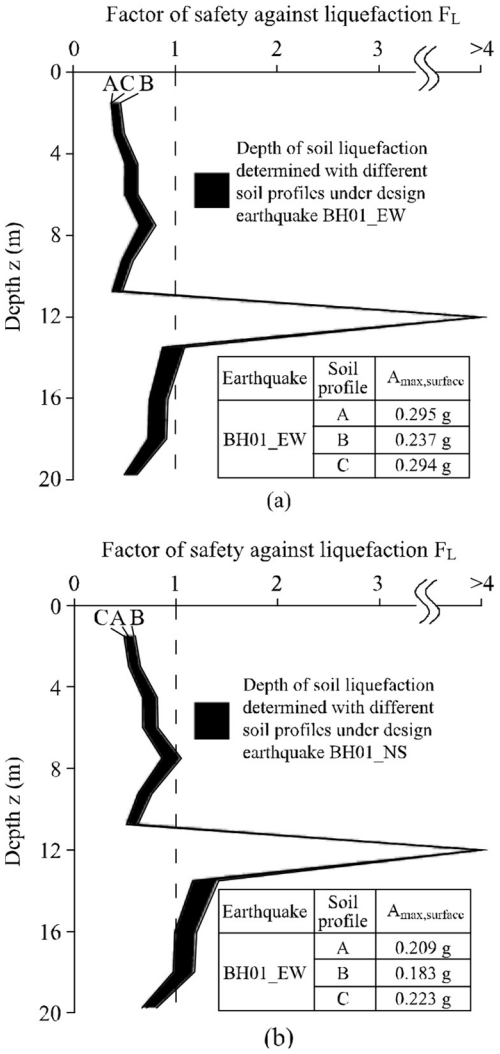

Fig. 14.Safety factor against soil liquefaction of BH01(TORI) determined using the NJRA method

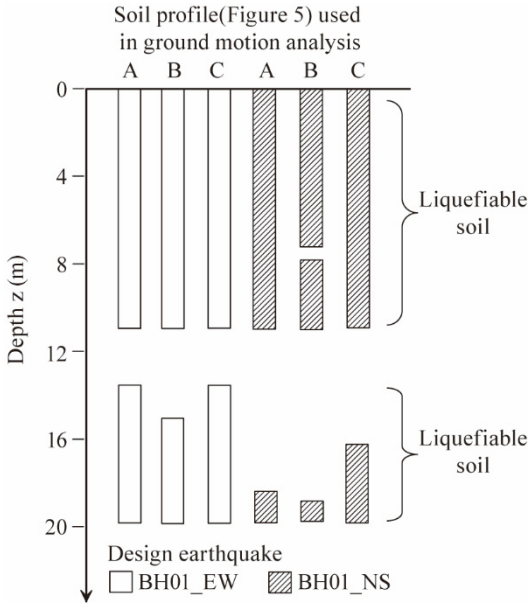

Fig. 15. Distribution of liquefiable soil layers of BH01(TORI) in the Changbin offshore wind farm determined using soil profiles with different simplified soil properties under design earthquakes

plified distribution of shear velocity along the depth engendered different responses at the seabed level. Hence, the shear velocity of soil is relevant to the determination of design seismic force in offshore wind foundation design.

VI. SOIL LIQUEFACTION POTENTIAL EVALUATION

During the development of offshore wind farms in Taiwan, evaluating the soil liquefaction potential of the seabed is essential. This study used the seismic acceleration time series at the bedrock (Fig. 8) and soil profiles of BH01(TORI), presented in Fig. 5, to conduct ground motion analyses. The PGAs described in Section V were used in the NJRA simplified empirical method to evaluate the soil liquefaction potential.

The soil liquefaction analysis results for BH01(TORI) are shown in Fig. 14. The results revealed that soil liquefaction may occur at a depth of more than 10 m in the seabed soil. The ranges of liquefiable soil layer differed for BH01_EW and BH01_NS. In foundation design, the worst case can be used. The range of liquefiable soil under he design earthquakes was also determined to be affected by the distribution of soil unit weight and shear wave velocity. Fig. 15 summarizes the depth of the liquefiable soil layer that was calculated using different simplified soil profiles in ground motion analyses. Notably, clay is normally treated as nonliquefiable soil. According to some studies, clayey soil with a low plastic index (PI) and high moisture content is still susceptible to soil liquefaction (cyclic mobility) (Bray et al., 2004; Bray and Sancio, 2006; Boulanger and Idriss, 2006). We observed only one thin clayey layer at a depth of 10.75–12 m at BH01(TORI); the PI value and moisture content derived for this layer suggested its susceptibility to soil liquefaction. Accordingly, we evaluated the liquefaction potential of this clayey layer.

The results in Fig. 15 present a high risk of soil liquefaction at BH01(TORI) in the Changbin offshore wind farm, Taiwan. When we performed the ground motion analysis to obtain PGAs for evaluating the soil liquefaction potential, the soil profile with a simplified distribution of shear wave velocity resulted in an underestimation of the PGAs as well as an underestimation of the thickness of the soil layers with the liquefaction potential. The geotechnical parameters obtained from the ground investigation provide crucial information for designing the foundations of offshore wind turbines. The shear wave velocity of soil in the design soil profile should be determined from field tests, such as PS logging, or from resonant

column tests in a laboratory when the soil liquefaction potential and seismic force are evaluated during the design of the foundations of offshore wind turbines in Taiwan.

VII. CONCLUSION

This study utilized the seismic response spectrum of the Changbin offshore wind farm seabed, Taiwan, that was proposed by Wang et al. (2016) to generate two sets of seismic acceleration time series of the bedrock (artificial earthquake BH01_EW and BH01_NS). The maximum bedrock accelerations of the two artificial earthquakes were determined to be 0.272*g*. One-dimensional seismic ground motion analyses results were used to determine the seismic acceleration time series at the seabed level. At BH01(TORI), an acceleration amplification factor of 1.085 was obtained under the designed earthquake BH01_EW, and an acceleration amplification factor of 0.768 was obtained under the designed earthquake BH01_NS.

A simplified profile of the shear wave velocity and the soil unit weight were considered in the ground motion analysis to evaluate the effects of soil uncertainties on ground motion responses during earthquakes. When the simplified profile of the shear wave velocity was used in the ground motion analysis, the PGA of the seabed was significantly underestimated. However, the simplification of the soil unit weight profiles did not affect the seismic acceleration time series at the seabed level. These results demonstrate the importance of soil shear velocities in ground motion responses analyses and validate that PS-logging tests or resonant column tests should be considered in the soil campaign during the development of offshore wind farms in Taiwan.

The PGAs of the Changbin offshore wind farm obtained from the ground motion analysis were used for soil liquefaction evaluation by using an SPT-N-based semiempirical method. The Changbin offshore wind farm was determined to have high soil liquefaction potential, and soil liquefaction could occur beneath the seabed surface up to a depth of 11–13 m. Soil liquefaction also occurred at soil depths greater than 13 m, and the thickness of the liquefied soil was determined to decrease with the PGA used. This study presents the scope of seismic demand, including ground motion analysis and seabed soil liquefaction potential analysis, for preparing the design basis of offshore wind foundations. The reduction factor of the peak shear stress in the direction of depth suggested by the NJRA method was used in this study. The distribution of the cyclic stress ratio along the depth may be contrary to the results obtained from the ground motion analyses. A modification of the reduction factor of the peak shear stress of soil can be considered using the results of ground motion analyses to obtain the A_{max} value of each depth for soil liquefaction analysis.

ACKNOWLEDGMENTS

The research was supported by the grants “Engineering databank and information modeling platform for offshore wind turbine foundation design and maintenance management (MOST 107-3113-E-006-011)”, the Ministry of Science and Technology of Taiwan.

REFERENCES

Athanasopoulos, G. A., P. C. Pelekis and E. A. Leonidou (1999). Effects of surface topography on seismic ground response in the Egion (Greece) 15 June 1995 Earthquake. Soil Dynamics and Earthquake Engineering 18, 135-149.

Andrus, R. D. and K. H. Stokoe II (2000). Liquefaction resistance of soils from shear-wave velocity. Journal of geotechnical and geoenvironmental engineering 126, 1015-1025.

American Petroleum Institute (2014). Seismic Design Procedures and Criteria for Offshore Structures. API RP 2EQ; American Petroleum Institute: Washington, DC, United States.

Construction and Planning Agency (2011). Seismic design specifications and commentary of buildings. Construction and Planning Agency, Taipei, Taiwan.

DNV/Risø (2002). Guidelines for Design of Wind Turbines, 2nd ed.; Jydsk Centraltrykkeri: Viby, Denmark.

Finn, W. D. L., R. H. Ledbetter and R. L. M. Fleming, A. E. M. Templeton, T. W. Forrest and S. T. Stacy (1991). Dam on liquefiable foundation: Safety assessment and remediation. Proceedings, 17th International Conference on Large Dams, Vienna, Austria, 531-553.

Hardin, B.O. and F. E. Richart (1963). Elastic wave velocities in granular soils. Journal of Soil Mechanics and Foundations Division 89, 33-65.

Hardin, B. O. and V. P. Drnevich (1972). Shear modulus and damping in soils: design equations and curves. Journal of Soil Mechanics & Foundations Division 98, 667-692.

Hardin, B. O. (1978). The nature of stress-strain behavior for soils. ASCE, Proceedings, Earthquake Engineering and Soil Dynamics, Pasadena, California, United States, 3-89.

Hashash, Y. M. A. and D. Park (2001). Non-linear one-dimensional seismic ground motion propagation in the Mississippi Embayment. Engineering Geology 62, 185-206.

Hashash, Y. M. A., M. I. Musgrove, J. A. Harmon, D. R. Groholski, C. A. Phillips and D. Park (2016). DEEPSOIL 6.1, User Manual.

Iwasaki, T. and F. Tatsuoka (1977). Effects of grain size and grading on dynamic shear moduli of sands. Soils and Foundations 17, 19-35.

Ishihara, K. and J. Koseki (1989). Cyclic shear strength of fines-containing sand. Proceedings, Discussion session on influence of local conditions on seismic response: 12th International Conference on Soil Mechanics and Foundation Engineering, Rio de Janeiro, Brazil, 101-106.

Ishibashi, I. (1992). Discussion of “Effect of Soil Plasticity on Cyclic Response” by Mladen Vucetic and Ricardo Dobry (January, 1991, Vol. 117, No. 1). Journal of Geotechnical Engineering 118, 830-832.

International Standard Organization (2004). Petroleum and Natural Gas Industries, Specific Requirements for Offshore Structures: Part 2: Seismic Procedures and Criteria; ISO 19901-2, International Standard Organization: Geneve, Switzerland.

Jaky, J. (1944). The coefficient of earth pressure at rest. Journal of the Society of Hungarian Architects and Engineers, 355-358.

Jamiolkowski, B. M. (1991). Design parameters from theory to practice, Theme Lecture. Proceeding of Geo-Coast'91, Yokohama, Japan.

Japan Road Association (1996). Specification for Highway Bridges, Part V, Seismic Design. Tokyo, Japan.

Koester, J. P. (1994). The influence of fines type and content on cyclic strength. ASCE. In Ground failures under seismic conditions, 17-33.

Kramer, S. L. (1996). Geotechnical earthquake engineering. Prentice Hall: New York, United States.

Kwok, A. O., J. P. Stewart, Y. M. Hashash, N. Matasovic, R. Pyke, Z. Wang and Z. Yang (2007). Use of exact solutions of wave propagation problems to guide implementation of nonlinear seismic ground response analysis

procedures. Journal of Geotechnical and Geoenvironmental Engineering 133, 1385-1398.

Massarsch, K. R. and B. B. Broms (1976). Lateral earth pressure at rest in soft clay. Journal of the Geotechnical Engineering Division 102, 1041-1047.

Olsen, R. S. (1997). Cyclic liquefaction based on the cone penetration test. Proceedings, NCEER Workshop on Evaluation of Liquefaction Resistance of Soils, Buffalo, New York, United States, 225-276.

Phanikanth, V. S., D. Choudhury and G. R. Reddy (2011). Equivalent-linear seismic ground response analysis of some typical sites in Mumbai. Geotech Geol Eng 29, 1109-1126.

Robertson, P. K. and R. G. Campanella (1985). Liquefaction potential of sands using CPT. Journal of Geotechnical Engineering 111, 384-403.

Robertson, P. K. and C. E. Wride (1998). Evaluating cyclic liquefaction potential using the cone penetration test. Canadian Geotechnical Journal 35, 442–459.

Seed, H. B. and I. M. Idriss (1970). Soil moduli and damping factors for dynamic response analyses. EERC 70-10, University of California, Berkeley, United States.

Seed, H. B. and I. M., Idriss (1971). Simplified procedure for evaluating soil liquefaction potential. Journal of the Soil Mechanics and Foundations Division 97, 1249-1273.

Silver, M. L. and H. B. Seed (1971). Volume changes in sands during cyclic loading. Journal of Soil Mechanics and Foundations Division.

Schnabel, P. B., J. Lysmer and H. B. Seed (1972). A computer program for earthquake response analysis of horizontally layered sites. EERC Report, University of California, Berkeley, United States.

Seed, H. B., I. M. Idriss, F. Makdisi and N. Banerjee (1975). Representation of irregular stress time histories by equivalent uniform stress series in liquefaction analyses. EERC 75-29, University of California, Berkley, United States.

Seed, H. B. (1979). Soil liquefaction and cyclic mobility evaluation for level ground during earthquakes. ASCE, Journal of the Geotechnical Engineering Division, 105, 201-255.

Seed, H. B., K. Tokimatsu, L. F. Harder and R. M. Chung (1985). Influence of SPT procedures in soil liquefaction resistance evaluations. Journal of Geotechnical Engineering 111, 1425-1445.

Seed, H. B. and P. De Alba (1986). Use of SPT and CPT tests for evaluating the liquefaction resistance of sands. ASCE, Use of in-situ tests in geotechnical engineering, Virginia, United States, 281–302.

Smoltczyk, U. (2001). Grundbau-Taschenbuch Teil 1. Geotechnische Grundlagen. Sechste Auflage.; Ernst & Sohn.

Tokimatsu, K. and Y. Yoshimi (1983). Empirical correlation of soil liquefaction based on SPT-N value and fines content. Soils and Foundations 23, 56-74.

Tokimatsu, K., S. Kuwayama and S. Tamura (1991). Liquefaction potential evaluation based on Rayleign wave investigation and its comparison with field behavior. Proceedings, 2nd International Conference on Recent Advances in Geotechnical Earthquake Engineering and Soil Dynamics, Missouri, United States, 357-364.

Taiwan Ocean Research Institute (2012). Field investigation and test analysis of drilling soils of Chang-Bin offshore area. Taiwan Ocean Research Institute, Kaohsiung, Taiwan.

Vucetic, M. and R. Dobry (1991). Effect of soil plasticity on cyclic response. Journal of Geotechnical Engineering 117, 89-107.

Wang, Y. K., J. F. Chai, Y. W. Chang, T. Y. Huang and Y. S. Kuo (2016). Development of seismic demand for Chang-Bin offshore wind farm in Taiwan Strait. Energies 9, 1036.

Yoshida, N (2015). Seismic ground response analysis. Springer: Dordrecht, Netherland.

APPENDIX

Soil data of borehole BH01(TORI) (TORI, 2012)

Layer	Depth (m)	Thickness (m)	Soil Type	SPT-N	γ_t (kN/m^3)	Moisture content (%)	Void Ratio	LL	PI
1	0.0~1.5	1.5	SP-SM	5	18.15	25.0	0.79	-	NP
2	1.5~3.0	1.5	SP-SM	7	17.46	24.8	0.85	-	NP
3	3.0~4.5	1.5	SM	10	18.05	25.4	0.81	-	NP
4	4.5~6.0	1.5	SP-SM	13	17.56	29.8	0.91	-	NP
5	6.0~7.5	1.5	SM	15	17.85	22.3	0.79	-	NP
6	7.5~9.25	1.75	SM	7	19.13	26.1	0.73	-	NP
7	9.25~10.75	1.5	SM	7	18.54	27.6	0.79	-	NP
8	10.75~12.0	1.25	CL	24	18.64	32.1	0.89	33	15
9	12.0~13.5	1.5	SM	25	19.52	23.5	0.64	-	NP
10	13.5~16.05	2.55	SP-SM	28	19.03	23.2	0.68	-	NP
11	16.05~18.0	1.95	SM	28	19.52	24.6	0.66	-	NP
12	18.0~19.75	1.75	SM	10	19.23	19.7	0.62	-	NP
13	19.75~21.0	1.25	SM	29	17.56	28.2	0.9	-	NP
14	21.0~22.5	1.5	SM	28	19.23	22.4	0.66	-	NP
15	22.5~24.0	1.5	SM	30	19.62	23.3	0.63	-	NP
16	24.0~25.75	1.75	CL	14	17.56	33.2	1.02	34	14
17	25.75~27.0	1.25	SP-SM	25	19.13	23.6	0.68	-	NP
18	27.0~28.5	1.5	SM	33	19.23	23.4	0.67	-	NP
19	28.5~30.0	1.5	SM	31	18.64	23.9	0.73	-	NP
20	30.0~31.5	1.5	SM	30	18.84	22.4	0.69	-	NP
21	31.5~33.0	1.5	CL	27	18.54	31.2	0.89	36	15
22	33.0~34.75	1.75	SM	33	19.62	22.0	0.62	-	NP
23	34.75~36.0	1.25	SM	34	19.42	21.5	0.63	-	NP
24	36.0~37.5	1.5	SP-SM	43	19.62	24.0	0.64	-	NP
25	37.5~39.0	1.5	SM	36	19.72	21.4	0.6	-	NP
26	39.0~40.75	1.75	SM	37	19.33	21.4	0.63	-	NP
27	40.75~42.0	1.25	SP-SM	31	19.33	24.4	0.67	-	NP

28	42.0~43.5	1.5	SP-SM	30	19.13	25.1	0.69	-	NP
29	43.5~45.0	1.5	SM	37	19.33	24.6	0.68	-	NP
30	45.0~46.75	1.75	SM	21	18.25	27.2	0.83	-	NP
31	46.75~48.0	1.25	SM	43	19.42	20.9	0.62	-	NP
32	48.0~49.5	1.5	SM	43	19.62	19.5	0.59	-	NP
33	49.5~51.0	1.5	SM	47	19.91	20.2	0.57	-	NP
34	51.0~52.5	1.5	SM	47	19.42	20.8	0.62	-	NP
35	52.5~54.0	1.5	SM	38	17.85	16.3	0.71	-	NP
36	54.0~55.5	1.5	SM	44	18.84	20.0	0.66	-	NP
37	55.5~57.0	1.5	SM	39	19.52	20.4	0.6	-	NP
38	57.0~58.5	1.5	SM	39	18.74	22.3	0.7	-	NP
39	58.5~60.0	1.5	SM	44	19.23	24.0	0.68	-	NP
40	60.0~61.5	1.5	CL	25	19.91	24.4	0.67	28	12
41	61.5~63.0	1.5	SM	46	19.23	21.7	0.65	-	NP
42	63.0~64.5	1.5	SM	43	19.03	22.0	0.67	-	NP
43	64.5~66.0	1.5	SM	37	20.70	17.0	0.48	-	NP
44	66.0~67.5	1.5	SM	43	17.85	20.7	0.76	-	NP
45	67.5~69.0	1.5	SM	42	20.01	18.1	0.55	-	NP
46	69.0~70.5	1.5	SM	46	21.09	16.3	0.44	-	NP
47	70.5~72.0	1.5	CL	28	18.93	26.1	0.74	32	14
48	72.0~73.5	1.5	SM	29	17.36	28.5	0.95	-	NP
49	73.5~75.0	1.5	SM	39	21.48	14.9	0.4	-	NP
50	75.0~76.5	1.5	SM	44	20.90	16.6	0.46	-	NP
51	76.5~78.0	1.5	SM	45	17.95	16.1	0.69	-	NP
52	78.0~80.0	2	SM	48	20.99	16.1	0.45	-	NP